GROUPEMENT POUR LE DEVELOPPEMENT
DE LA TELEDETECTION AEROSPATIALE

IGN - CNES - IFP - BRGM

JOURNEES DE TELEDETECTION
DU G.D.T.A.

ST-MANDE 21-23 SEPTEMBRE 1977

UTILISATION DES SATELLITES
EN TELEDETECTION
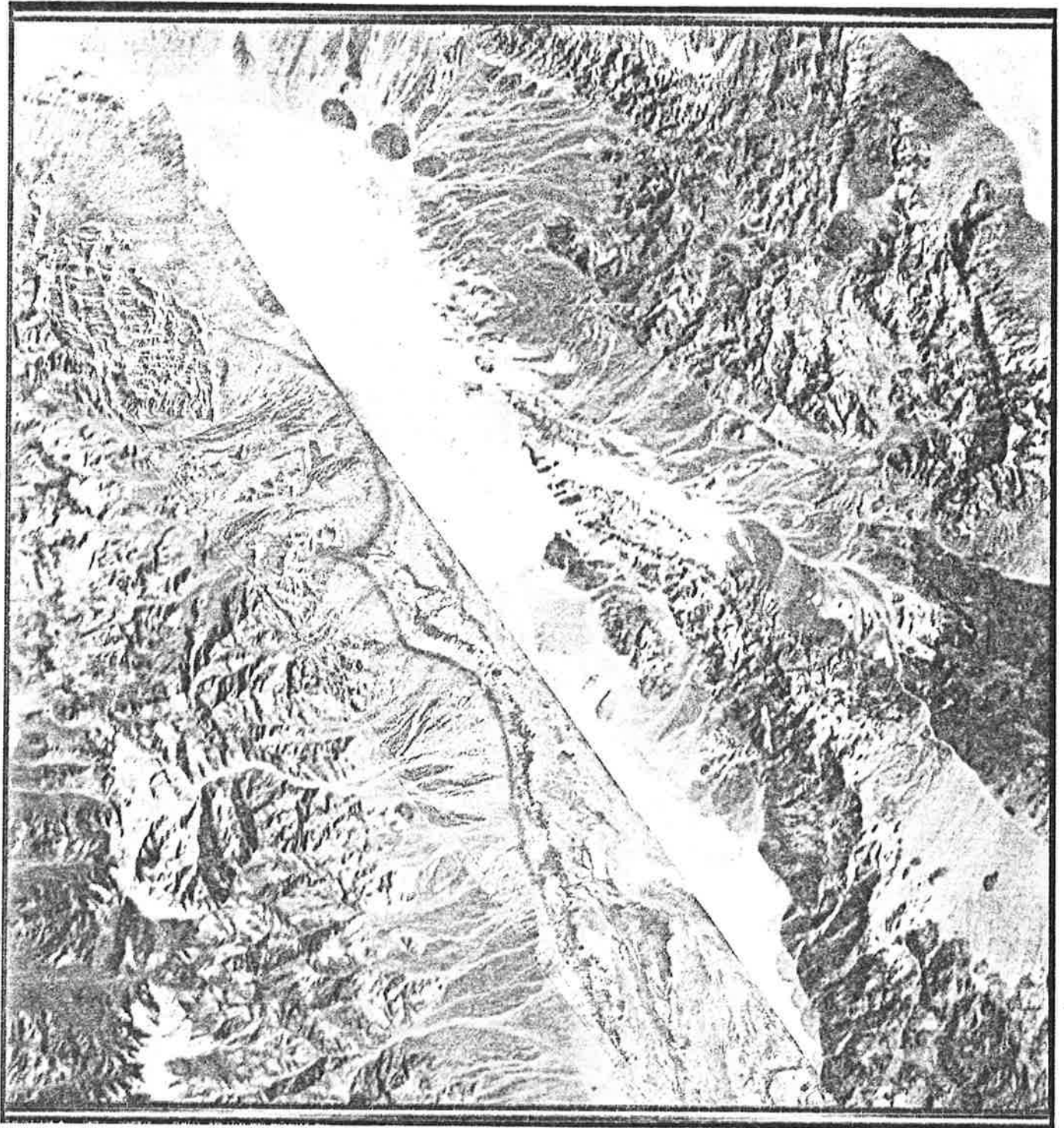
IGN - CNES - IFP - BRGM

Figure 14: Composite of Landsat and airborne L-band radar images of Death Valley, California: Landsat (red), radar - VH - polarized (green), radar- VV - polarized (blue).
Image registration and color coding by digital image processing (Image Processing Laboratory of the Jet Propulsion Laboratory).

MAPPING WITH SATELLITE SIDE-LOOKING RADAR[+]

Franz Leberl

Technical University Graz, Austria

and

Charles Elachi

California Institute of Technology, Jet Propulsion Laboratory

Pasadena, California, USA

Abstract:

Satellite radar imaging has become a reality as a by-product of the Apollo 17 Lunar Sounder Experiment in 1972. Presently research efforts are being undertaken in preparation of future satellite radar mapping projects (SEASAT-A, Space Shuttle, Spacelab, Venus Orbital Imaging Radar). Planning for acquisition and application of the satellite images depend, among others, on a number of radargrammetric considerations to be discussed in this paper. Questions of single image geometry and radar stereo viewing precede a review of major geoscience applications of satellite radar images. These are presently seen to be in oceanography (ocean waves), glaciology (sea-ice), geology/planetology and general purpose mapping.

Resumé:

Les images radar de satellite, apparues comme sous-produit de l'expérience de sonde lunaire du vol Apollo 17 en 1972, sont dès lors devenues une réalité. Actuellement des efforts de recherche sont entrepris pour la préparation des futurs projets de cartographie par radar de satellite (Seasat A, Space Shuttle, Spacelab, Venus Orbital Imaging Radar).

Le calendrier de l'acquisition et de l'utilisation des images dépend, entre autres, d'un certain nombre de considérations radargrammétriques qui sont discutées dans cette présentation. Des questions de géométrie d'images simples et d'observation stéréoscopique radar sont présentées, suivies par une revue des applications principales des images radar dans les sciences de la terre.

L'océanographie (vagues), la glaciologie (marine), la géologie/planétologie et la cartographie au sens large paraissent être actuellement les applications principales.

1. INTRODUCTION

The Apollo 17 Lunar Sounder Experiment has, among other data, resulted in the first satellite side-looking radar images (Phillips et al., 1973). Since then efforts have continued towards development of radar imaging systems to be put into orbit around the Earth and the planet Venus.

The acquisition and application of satellite radar images is influenced by radargrammetric considerations. In the present paper, such considerations will be reviewed with respect to single images and stereo mapping. This is preceded by a discussion of features that are unique to satellite radar.

Practical results have been obtained with lunar satellite radar (Elachi, et al, 1976). Examples of this work will be discussed in this paper where appro-

priate. As a preparation for future orbital radar missions (Seasat-A, Space Shuttle Payload, Spacelab, Venus Orbital Imaging Radar (VOIR)) work is presently being carried out with airborne images to study and illustrate potential applications. Examples presented in this paper will concern geology, oceanography, radargrammetric mapping, and sea ice study.

2. SATELLITE RADAR

High resolution radar imaging from a satellite must be with a synthetic aperture, since ground resolution would be comparatively coarse with a real aperture. In the synthetic aperture radar the orbit height is a much less significant parameter than in optical imaging as far a image resolution and scale is concerned. The radar system is measuring distances between the antenna and the object with an accuracy independent from the distance itself. This basic fact is illustrated in Figure 1: Radar ground resolution can be the same irrespective of orbit height.

The width of an area covered by a single orbital radar imaging pass (swath width) depends, among a series of other constraints, on the number of resolution cells that the recording and image correlation system can display. This may be as many as, for example, 2000 cells. To cover a wide area, several recording units are required. The swath width is thus rather a function of resolution, not of orbit altitude. To cover a given swath satellite radar will have much smaller variations of incidence angles (elevation angles) than airborne radar. Therefore, an object appears to be more uniformly illuminated from near to far range. Also, the radar layover and shadows can be more efficiently optimized when the range of incidence angles is small.

One may thus conclude that orbit altitude only defines the range of incidence angles for imaging a specified swath. These angles affect then the conversion of range resolution into resolution on the ground, denoted by a_g (Figure 2). For a given range resolution, the ground resolution deteriorates with steeper look-angles; these, in turn, have also a significant effect on the geometry of the single image and the stereo pair.

A comparison of satellite and airborne radar shows that advantages of one over the other are essentially those also encountered with other methods of imaging: the foremost ones are the near-instantaneous coverage of large areas (satellite velocity is 7 km/sec. versus 0.2 km/sec. for aircraft) and the reduced variable cost of repeated satellite imaging of the same area. The main reasons to apply radar in conjunction with, or instead of, other sensing techniques are the penetration capability (atmosphere, clouds, rain, snow, vegetation, etc.) and the fact that radar provides its own illumination (is therefore independent of sun, time of day). These advantages of radar have led to its wide-spread application in many operational projects (Roessel, et al., 1974).

In addition, there are some characteristics of radar whose potential to earth science applications have not yet been entirely explored: polarization, choice of illumination angle, multi-frequency capability, sensitivity to object surface roughness and to variations of dielectric constant, on-line image telemetry, etc. Efforts to study these characteristics and the usefulness of radar for earth science applications are presently intensifying.

3. GEOMETRIC PROPERTIES OF A SINGLE SATELLITE RADAR IMAGE

3.1 Visual Appearance of a Radar Image

Figure 3 presents an example of a satellite radar image taken in orbit around the Moon from an altitude of about 116 km. The wavelength is 2 m. Imaging is with elevation angles off nadir between $0°$ and $20°$, thus from the nadir out
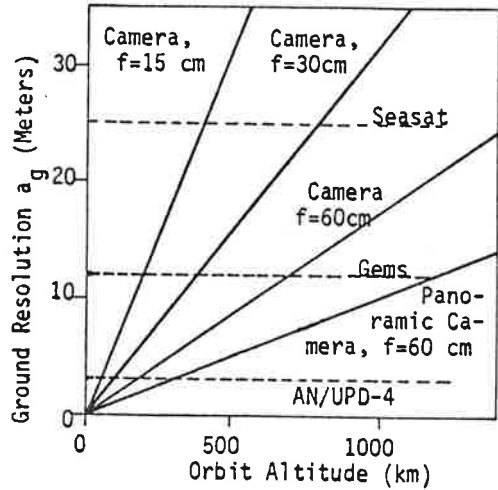
452

Fig.1: Resolution of cameras and synthetic aperture radars as function of orbital altitude.
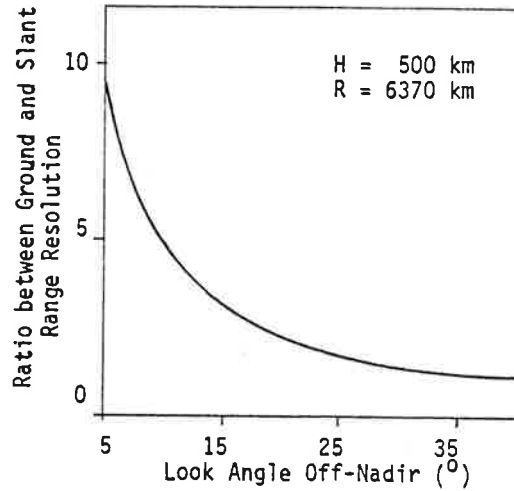

Fig.2: Slant and ground range resolution versus look angle off nadir. R... Planetary radius, H... Height.
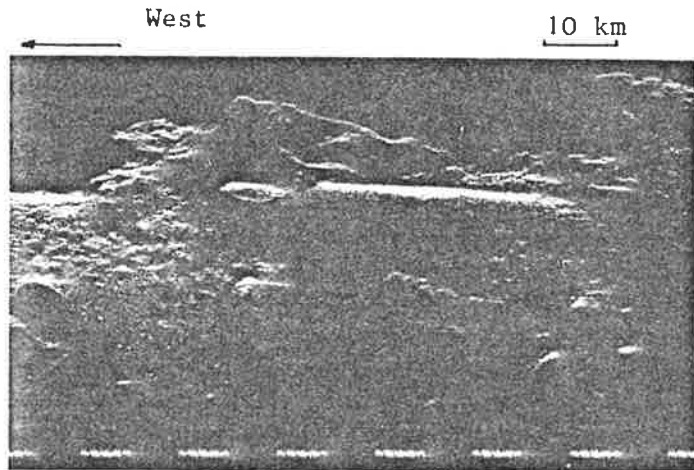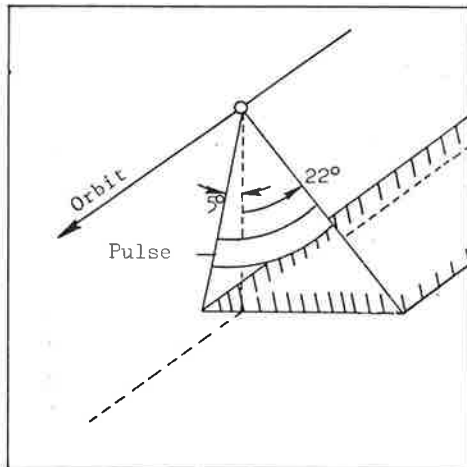

Figure 3: Example of Apollo 17 Lunar Sounder Experiment (ALSE) side-looking radar image and imaging arrangement.
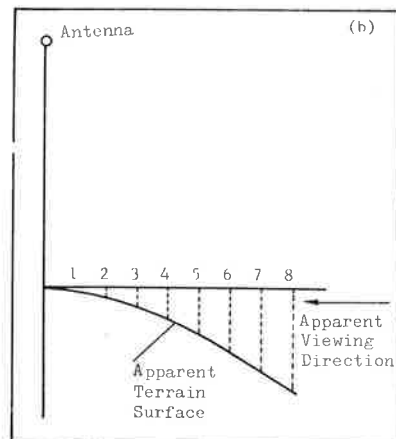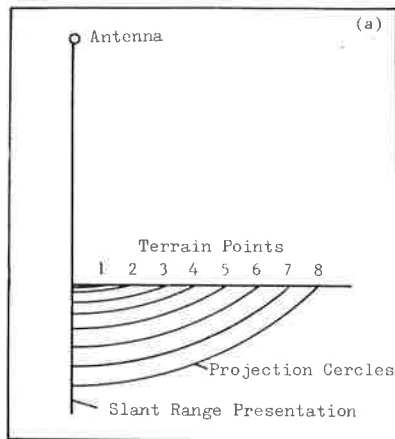

Figure 4: Explanation of the panoramic visual effect when viewing a radar slant range presentation.

453

to the side of the satellite track. The lunar surface seems to be rolled onto a cylinder. This is caused by the slant range display. The same effect is also obtained with airborne radar and is particularly striking in the nadir area. Figure 4 provides an explanation for the visual appearance of the image in Figure 3: the slant distances r between antenna and objects are presented as cross-track image coordinates. This may also be explained by stating that the projection lines connecting object and image points are concentric circles around the antenna position (in a central projection, the projection lines are straight and intersect in the perspective center).

Since points in the area of the nadir have all nearly the same distance from the antenna, this area is compressed in the image leading to the noted panoramic visual impression. The equation

$$r^2 - Y^2 = H^2 \tag{1}$$

relates orbit height H to slant range r and cross-track object coordinate Y. For a given value of H this presents a hyperbola with its point of symmetry at r = 0 (antenna). Rectification can be accomplished by displaying as the cross-track coordinate the distance

$$Y = (r^2 - H^2)^{1/2} \tag{2}$$

An example of such rectification is shown in Figure 5. It presents a true orthographic presentation of the imaged object only to the extent that H is known and that there are no secondary perturbations of image geometry present. In the case of a non-flat surface, height differences evidently may result in relief displacement and shadowing. This has been described at length in the radar literature (e.g., Manual of Photogrammetry, 1966, Rydstrom, 1968; Leberl, 1975) and will not be repeated here.

3.2 Projection Properties of Radar Images

Figure 6 presents sample computations for the scan lines of an orbital radar which is assumed to be at $30°$ latitude, $0°$ longitude and at 800 km altitude. It illustrates that there are a number of phenomena which may cause a satellite radar image to systematically differ from the geometry of map projections. A number of corrections must be applied in the image formation. Systematic geometric image deformations would be present if:

- the cross-track dimension of the image represented slant range;
- the slant ranges were corrected to ground ranges using Equation (2), but planetary curvature was not considered;
- the along-track dimension showed the effects of squint (correlation of the synthetic radar signals with respect to a non-zero doppler frequency);
- the image showed effects of the planetary revolution.

Radargrammetric work with satellite images can have high relative accuracy (distances and angles). The absolute accuracy (of determining point coordinates from the radar images) depends largely on the accuracy with which the orbit can be determined and the extent to which it is being applied for radargrammetry (Tiernan, et al., 1976; Leberl, 1976b). Concluding from experiences gained in work with LANDSAT imagery and other types of satellite data, one must expect higher relative than absolute accuracy.

The practical results of satellite radargrammetry using Apollo 17 data taken over Crater Maraldi and Mare Serenitatis showed that the images had absolute errors of up to several kilometers. Distances, however, could be determined with errors of about ± 200 m. It should be noted that the raw images were not corrected geometrically. All corrections had to be applied in the radargrammetric data reduction. The values are not representative of mapping accuracies to be expec-

Original image

Geometrically rectified

5 km

Figure 5: Radar slant range presentation and digitally rectified radar image, taken with L-band SAR at 10 km flight height of an area in Northern Alaska.
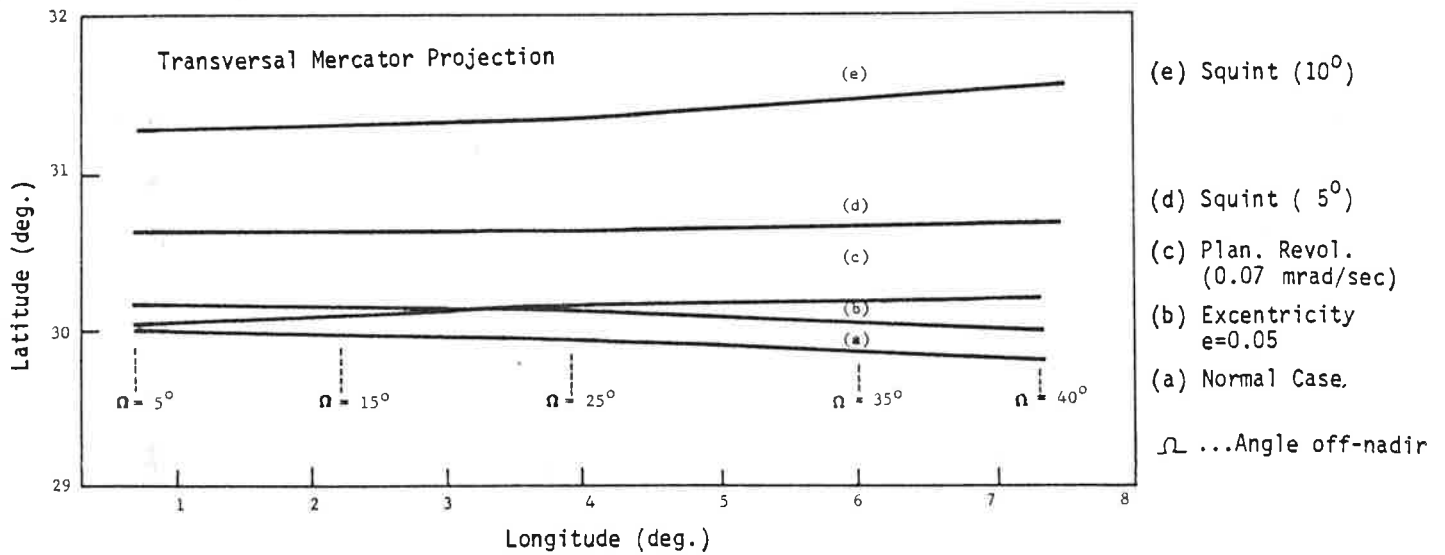

Figure 6: Sample computation for orbital side-looking radar scan lines on planetary surface. Sensor at 30° latitude, 0° longitude, 800 km altitude.
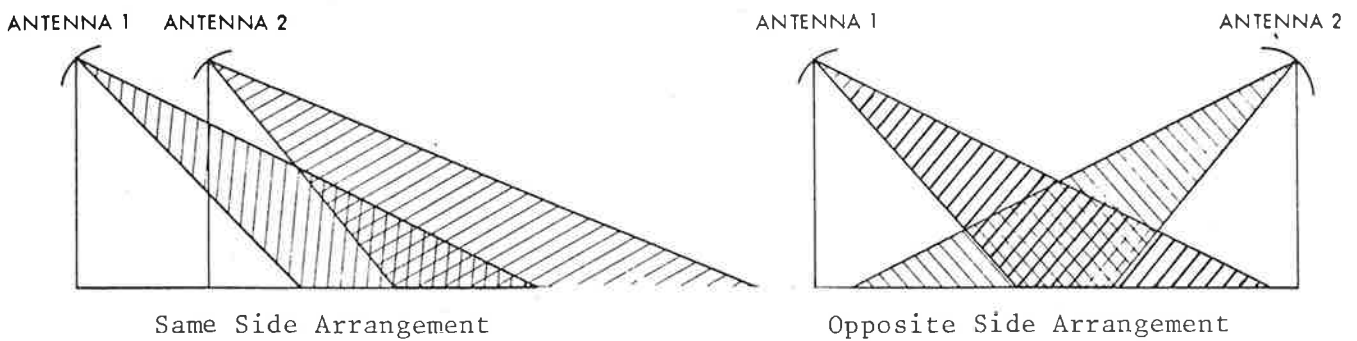

Figure 7: Same side and opposite side arrangements for stereo radar.

455

ted in future orbital radar projects. Such accuracies can be higher due to superior resolution, accuracy of satellite tracking and system calibration.

4.   RADAR STEREO MAPPING

4.1 Visual Radar Stereo

Stereo viewing of overlapping radar imagery can greatly enhance the interpretation of the images by providing an improved means to observe morphological details, to determine slope angles and height differences and to improve cartographic mapping and point positioning accuracies.

With synthetic aperture radar relief displacement is always in cross-track direction (at 90° to the nadir line). Therefore, overlapping images can produce a three-dimensional visual stereo model only with two schemes (Figure 7): same-side and opposite-side (LaPrade, 1963; Rosenfield, 1968). Another scheme with cross-wise intersecting orbits does not seem to permit visual stereo (Graham, 1975). Other types of stereo arrangements would only be possible with real aperture radar, for example with convergent schemes using tilted antennas (Leberl, 1972; Bair and Carlson, 1974).

In order to view a three-dimensional model, the two images of the stereo pair must be sufficiently similar: the image quality and object illumination must be comparable and the geometric differences (stereo parallaxes) must not exceed a certain maximum. In photography this hardly ever presents a problem since the sun angles do not chance drastically in overlapping photos. However, in radar images the illumination angles depend on the sensor position and so does the appearance of the images.

Figures 8 to 11 present examples of radar stereo pairs demonstrating some of the limits to stereo viewing. Figure 8 shows part of the Estrella mountains in Arizona, USA, imaged with an opposite side arrangement from an aircraft at 12 km altitude. It can be clearly seen that slopes that reflect strongly in one image are in the radar shadow in the other image. A stereo impression can be obtained in the flat areas of this stereo pair but becomes very difficult in the mountains. Figure 9 demonstrates a same side stereo pair taken with the same radar system. Stereo viewing does not present any problems. Koopmans (1973) could show in one experiment in Colombia, with this type of stereo, that in certain cases drainage analysis was superior to that from available aerial photography.

Figures 10 and 11 present two Apollo 17 satellite radar stereo pairs taken of the lunar surface with same side geometry and very small stereo base. However, look-angles are steeper than those in Figures 8 and 9. This leads to larger relief displacements and differences of image content in the stereo mates even with a small stereo base. In the flat parts of Figure 10 stereo viewing is not difficult. However, in the Apennin mountains stereo fusion becomes nearly impossible. This is even more so in Figure 11 taken over the rugged Oriental region.

From the above examples the following factors influencing radar stereo viewing can be identified:

    Stereo arrangement (same-side, opposite-side);
    Look-angles (angles off-nadir);
    Stereo intersection angles;
    Ruggedness of the terrain.

The exact limits of radar stereo and the interrelation among the above factors are presently not well understodd. Apart from an effort described by LaPrade (1970) research has in the past not dealt with visual stereo but with the geometry of intersecting radar projection circles. In addition, LaPrade (1970)
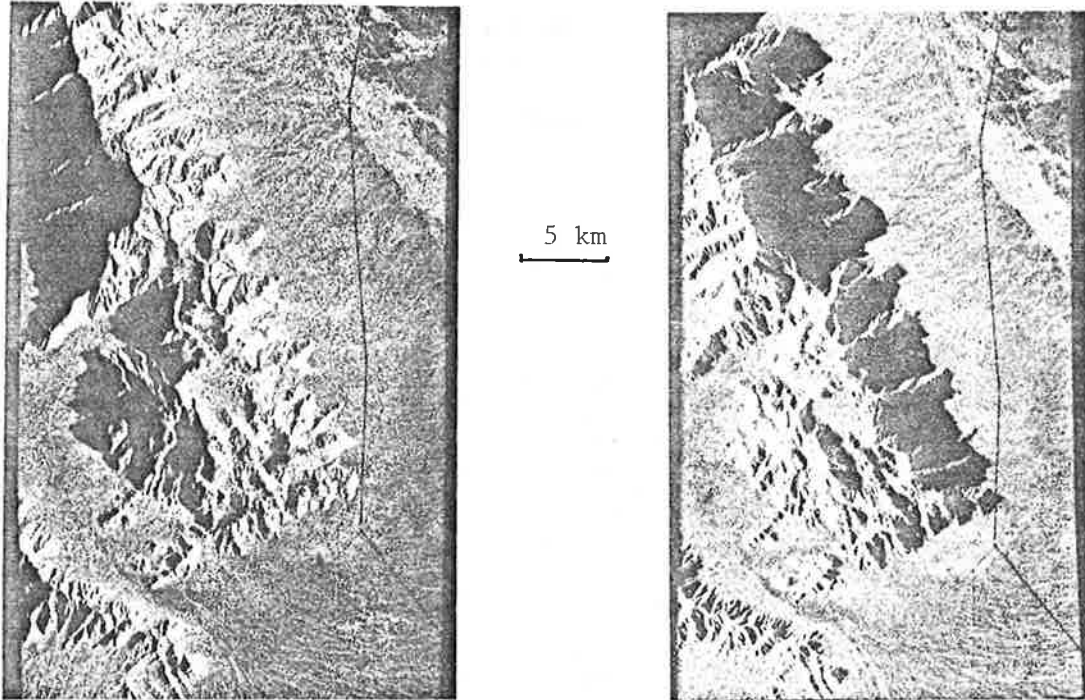
Figure 8: Opposite side radar stereo with airborne SAR of the Estrella mountains in Arizona, USA (courtesy of Goodyear Aerospace - Litton Aeroservice).
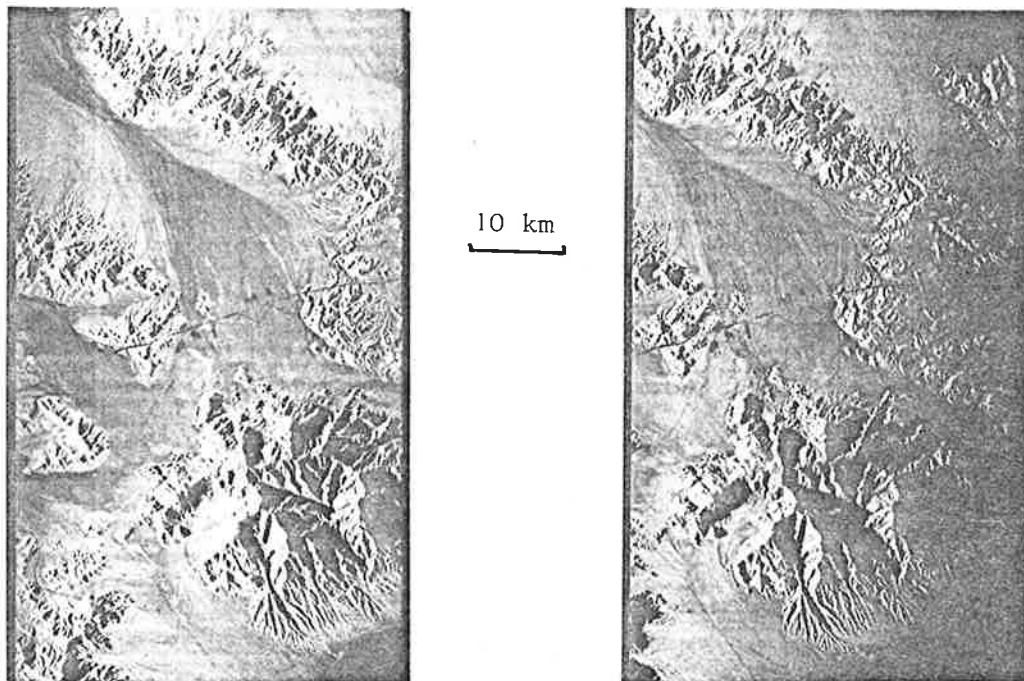

Figure 9: Same side radar stereo with airborne SAR of an area near Needles, California, (Courtesy of Goodyear Aerospace - Litton Aeroservice).
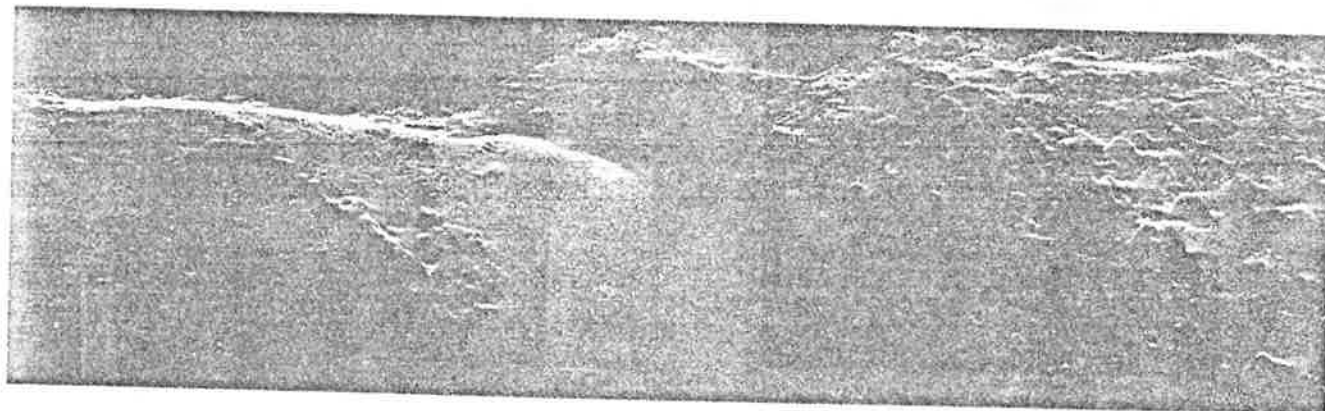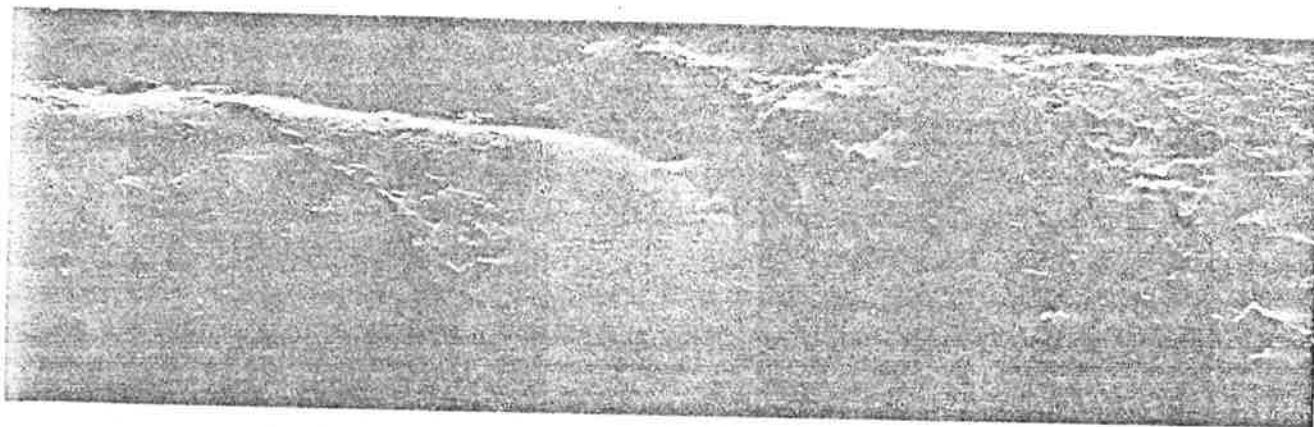
Figure 10: Same side stereo with lunar Apollo 17 SAR of the Appennin region. ⌞————⌟ 10 km
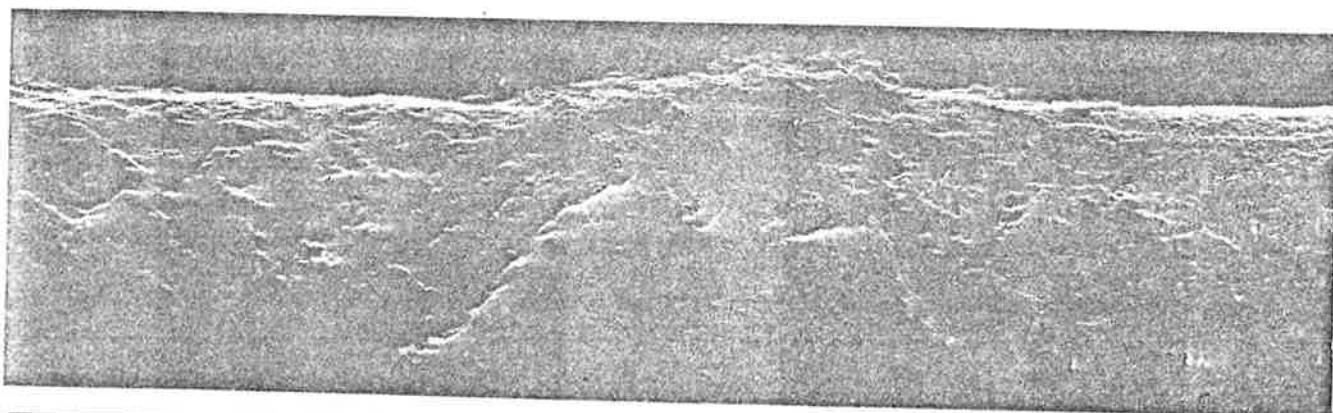

Figure 11: Same side stereo with Apollo 17 SAR of the Oriental region on the moon. ⌞————⌟ 10 km

concentrated on stereo viewing of man-made features and small objects, not of terrain features.

Past experiences lead to the tentative conclusion that opposite-side stereo can only be applied in cases of flat or rolling surfaces, while rugged terrain requires same-side imaging. Stereo viewing improves with shallower look-angles ($45°$ off nadir and more). With steeper look-angles (near nadir) the stereo base has to reduce for successful stereo viewing, thereby leading to less accuracy.

4.2 Accuracy and Geometry of Radar Stereo Models

From orbit the swath will be covered with a rather small range of viewing angles (from 800 km altitude, a 100 km swath can be imaged with a $5°$ range of look-angles). Therefore, an extremely small stereo-basis and poor intersection geometry are obtained using same-side geometry with 60 % overlap. Figure 12 provides results on the accuracy of a stereo model where Y is the cross-track and Z the height coordinate. Given a $3°$ intersection and a root mean square error of range of $\pm$ 10 m, several hundred meters of Y- and Z-errors will be obtained. However, accuracies improve rapidly with larger intersection angles. With aircraft radar, a frequently used stereo intersection angle is $15°$ and that seems to provede valuable stereo. To obtain such large stereo angles from orbit, the look-angles in the two orbital stereo passes have to be different (Figure 13).

Viewing the lunar orbital stereo pairs, such as Figures 10 and 11, shows that also in the stereo model the surface seems to be rolled onto a cylinder (Phillips, et al., 1973). It can be confirmed algebraically that the stereo model has a 4th-order cylindrical bow (Leberl, 1976a). This could be avoided if images were presented with corrected cross-track coordinates ("ground range presentation"). However, the observed model heights would still have to be converted to object heights using parallax formulas that differ from those used with photography. Such formulas have been published by many authors (e.g. Koopmans, 1974; Derenyi, 1975; Leberl, 1975).

Actual results on stereo mapping with orbital radar were obtained with the lunar Apollo 17 data (Leberl, 1976b). From a 116 km altitude, the stereo base was 3 km, the intersection angles amounted to about $2°$. The root mean square height error amounted to $\pm$ 100 m, and across-track coordinate errors to about $\pm$ 500 m. This confirms theoretically derived predictions that were illustrated in Figure 12.

5. MAPPING APPLICATIONS

5.1 Geology/Planetology

Airborne imaging radars have been widely used by oil and exploration companies for reconnaissance surveys of potential sites of mineral deposits and for geologic mapping. There are two kinds of information that can be extracted from radar images. Radar images are used in a way similar to photography to extract morphological information. They show topographic features, lineaments, texture, vegetation lines, drainage patterns and fault scarps (Dellwig and Moore, 1966; Schaber, et al., 1976; Wing 1970; Wing and Dellwig, 1970; Wing, et al., 1970).

The second kind of information is a result of the fact that the radar backscatter (i.e., brightness on the image) is directly related to the surface roughness and dielectric constant. A quantitative measurement of the brightness in calibrated radar images allows the classification of a region in different categories of backscattering units. In cultivated regions, these different back-
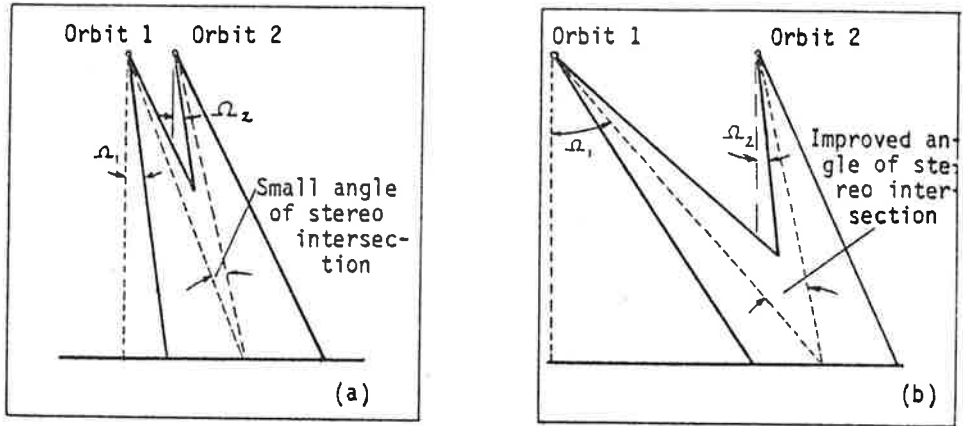
Figure 12: Range of incidence angles relates to swath width and orbit altitude: (a) 60 % overlaps, fixed imaging arrangement; (b) stereo with modified look angles in the two orbits.

Figure 13: Accuracy of a same side satellite stereo radar, expressed in root mean square errors σ_y of the cross track coordinate (a); and of height σ_z. ($\Delta\Omega$ is the intersection angle, Ω the look angle off-nadir).

~5 km

Figure 15: Radar image of ocean waves, taken at L-band from an altitude of 10 kilometers.

backscattering units (Schaber, et al., 1976) correspond to areas with different vegetation coverage (i.e., type of veget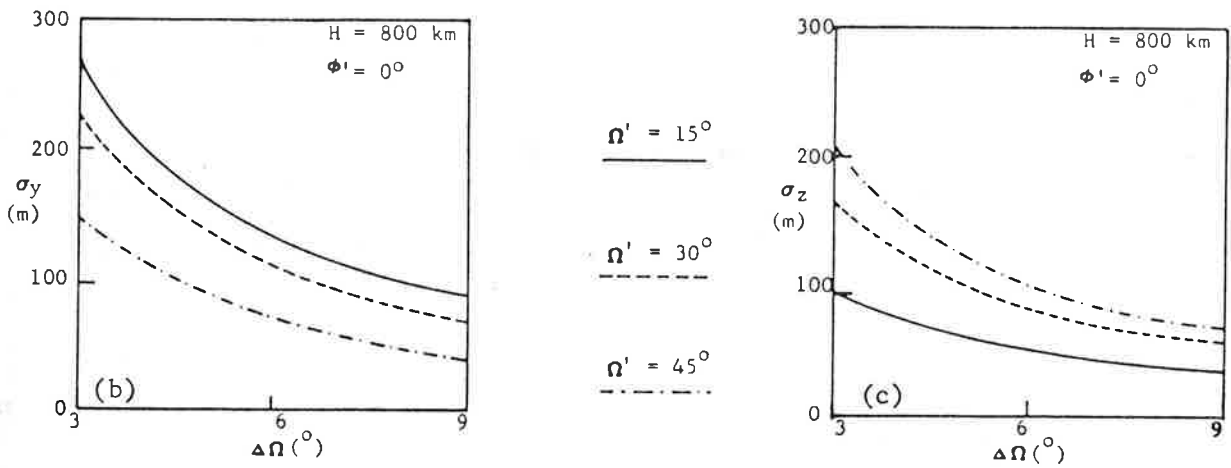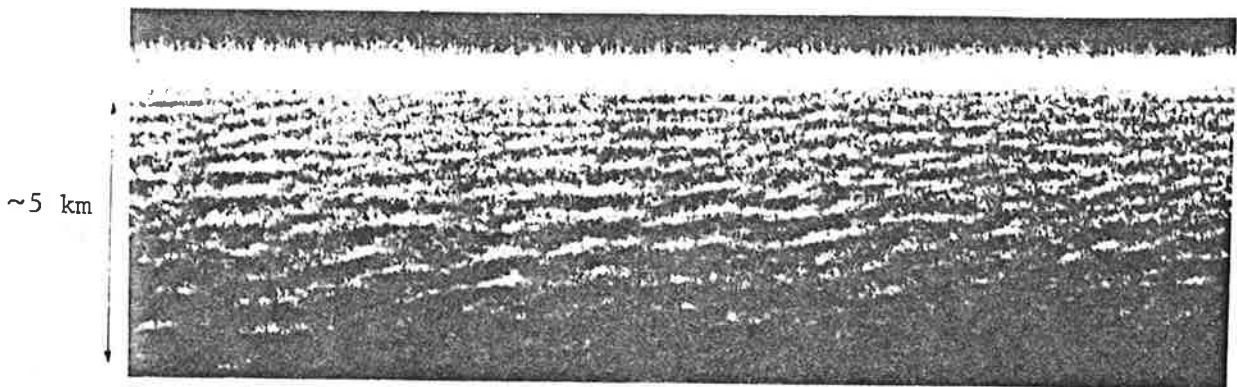ation or stage of vegetation growth) or different soil moisture. In arid regions, these backscattering units correspond mostly to regions of different roughness. The complementary use of the morphologic and roughness information goes an appreciable way in understanding the surface geology.

Radar imagery can thus provide unique information on the surface geology. The most unique features of radar have been mentioned before (all-time, all-weather sensor). The experimentor has complete control over the illumination angle, which can be selected depending on the type of experiment. Geologic mapping is better accomplished with large incidence angles (look-angles off-vertical) to enhance topography, while soil moisture mapping requires small incidence angles to minimize the effect of small scale roughness.

The dependence of the image brightness on the surface roughness (on the scale of the radar wavelength, i.e., from a few millimeters to a few tens of centimeters) also sets radar apart from visible and IR imagery whose brightness depend on the spectral reflectance (or emittance) of the surface (in the wavelength region of a fraction of microns to a few tens of microns). Thus, the combination of multi-spectral radar. IR and visible imagery can provide new information that may not be extracted from one type of imagery alone. Research is just starting in the area of interpretation of multispectral radar/IR/visible. Figure 14 shows L-band airborne radar imagery digitally registered to LANDSAT imagery of Death Valley in California. False colors are used to facilitate the analysis. However, actual experiences with interpretation of multi-sensor image composites are not yet available in the literature.

A number of Earth orbiting experiments on the Shuttle (OFT-2 in 1979) and on Spacelab (flight in 1982) are planned by NASA to evaluate the use of imaging radars for geologic mapping. These experiments will be used to define an operational free flyer for global mapping.

The techniques developed in the interpretation of radar imagery of the Earth will be the basis for interpreting the data obtained with planetary orbiting radar. The specific case in question is the Venus Orbiting Imaging Radar (VOIR) mission which is under consideration by NASA for a 1983 launch. The surface of Venus is hidden behind a global cloud cover. The only information on the surface topography was obtained using Earth-based radar, which provided low resolution (i.e., many kilometers) over a small percentage of the surface. The VOIR sensor will provide global mapping of the Venusian surface with resolution better than a few hundreds of meters.

5.2 Oceanography

In 1978, the Seasat-A satellite will be put into near polar orbit with an imaging radar onboard. The main objective of the radar experiment is to map the ocean surface and provide all-weather/all-time global information on wave patterns, sea surface features (such as currents) and polar ice features (see Section 5.4).

Airborne radar imagery of a variety of ocean surface features have been reported in the literature. Ocean waves have been imaged under a variety of conditions from relatively calm seas to hurricanes (Brown, et al., 1976; Larson, et al., 1976; Elachi and Brown, 1977; Elachi, 1976, 1977; Shemdin, et al., 1976; Elachi, et al., 1977). Internal waves (Elachi and Apel, 1976), current boundaries (Larson, et al., 1976), weather fronts, eddies and ship wakes (Brown, et al., 1976) have also been observed.
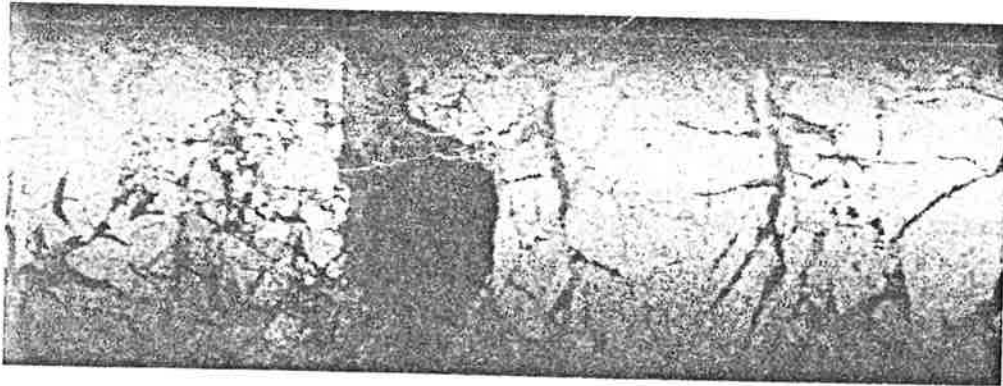
In the case of ocean surface waves, the radar image is representative of variations of the coherent radar backscatter cross-section, which in turn is
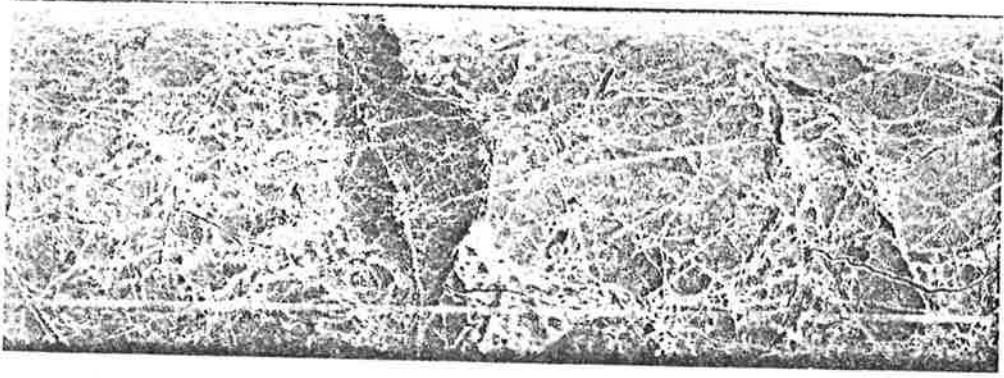
Figure 16: Examples of sea ice imaged by airborne radar (a) in April 1976, using L-band; (b) same as (a), but with X-band; (c) imaged in August 1975; (d) imaged in October 1975, using L-band radar.

462

dependent of the local slope, orbital velocity, phase velocity and small scale roughness. The exact mechanism of image formation is not well understood. However, experimental measurements verified that the radar image gives the wavelength and direction of the ocean waves (Figure 15). Some techniques are also being tested to derive the wave heights from the radar image (Jain, 1977).

Evidently, also in oceanographic applications, one of the most attractive features of the radar is its all-weather capability. This was clearly illustrated when imaging of wave patterns was obtained under hurricane Gloria in 1976, using the JPL (Jet Propulsion Laboratory - California Institute of Technology) airborne imaging radar (Elachi, et al., 1977).

5.3 General Purpose Land Mapping

National topographic mapping tasks generally appear to lag behind demand. In less developed regions of the world this applies to basic mapping, while in industralized countries the bottleneck is in the revision of existing topographic maps. A mapping application of satellite radar data may be in remote regions where, thus far, airborne radar has found a task (areas of tropical rain forest). This may apply to small scale planimetric mapping, to map revision and - in exceptional cases - to height mapping. Applications in industrialized countries have not been explored. Radar may have to compete in this task with satellite photography which, in the age of the Space Shuttle, may be expected to be available to a much greater extent than in the past.

5.4 Sea and Lake Ice

Monitoring sea and lake ice, as well as icebergs, is a task that can successfully be carried out with radar (Schertler, et al., 1975; Super, et al., 1975; Campbell, et al., 1976). Since arctic regions are often cloud covered or not well illuminated by the Sun, this makes radar a tool well suited for the ice monitoring task. Figure 16 presents examples of synthetic aperture radar images at L-band (25 cm wavelength) and X-band (3 cm) of arctic sea ice taken from an airplane at an altitude of 10 km during spring, summer and fall (note the differences of images 16a, b in X- and L-band due to greater surface penetration of L-band). In an ice mapping study, using such images taken at different times, the overall ice drift could be measured with an absolute accuracy of about $\pm$ 2 km and relative ice motions within one image were found in error for about $\pm$ 0.1 km (Leberl, et al., 1976). It is expected that accuracies obtained from satellite radar would be better than those obtained from aircraft data since orbit stability is higher and the swath is wider in proposed satellite projects.

5.5 Other Earth Science Applications

There are numerous other potential applications of radar imagery which are at different levels of maturity. Of high importance appears to be the use of radar for measuring soil and snow moisture content, identifying vegetation types and assessing vegetation health. The level of experiments is still at a stage where truck mounted radars and airborne scatterometers are being used. These indicate, however, that there is a great potential for radar in the above mentioned applications. Imaging radar has also been investigated for land use and urban mapping (Bryan, 1975).

6. CONCLUSIONS

Research on earth science applications of radar images seems to have been intensified recently, after a period in which efforts were largely concentrated on satellite scanning. This may be, in part, caused by opportunities that may be derived from satellite radar mapping projects that are presently being pro-

posed in the U.S.A. The main thrust is in oceanographic and sea ice applications, but efforts also aim at uses of satellite radar images in geology/planetology, general purpose and vegetation mapping.

The main advantages of radar are its penetration capability (e.g., clouds) and its active mode of operation (day and night imaging). Other characteristics (polarization, choice of look-angles, etc.) may contribute to applications of radar in conjunction with, or instead of, images obtained from different sensors. Such characteristics are reviewed in the paper with respect to major applications. This is preceeded by a discussion of radar image geometry and stereoviewing concerning visual appearance and accuracy of the image and stereomodel. Stereo interpretation of radar may be a valuable asset in the mapping of cloud-covered planet Venus in a radar mission planned for 1983.

REFERENCES:

Bair, L.G. and G.E. Carlson (1974) "Performance Comparison of Techniques for Obtaining Stereo Radar Images," IEEE Trans. on Geoscience Electronics, GE-11.

Brown, W.E., C. Elachi and T.W. Thompson, "Radar Imaging of Ocean Surface Patterns", J.Geophys.Res., Vol. 81, pp. 2657-2667, 1976.

Bryan, M.L., (1975) "Interpretation of an Urban Scene Using Multi-Channel Radar Imagery", Remote Sensing of Environment, Vol. 4, No. 1, pp. 49-66.

Campbell, W.J.; P. Gloersen; R.O. Ramseier and C. Elachi (1977) "Simultaneous Passive and Active Microwave Observations of Near-Shore Beaufort Sea Ice," Presented at the 9th Annual OTC, Houston, Tex., May 2-5, 1977.

Elachi, C., 1976, "Wave Patterns Across the North Atlantic on September 28, 1974 from Airborne Radar Imagery," J. Geophys. Res., 81, 26.

Elachi, C. and Apel, J., 1976, "Internal Wave Observations Made with an Airborne Synthetic Aperture Imaging Radar," Geophys. Res. Lett., 3, pp. 647-650.

Elachi, C. and Brown, Jr., W.E., 1977, "Models of Radar Imaging of the Ocean Surface Waves," IEEE Trans. on Antennas and Propagation, AP-25, pp. 84-95.

Elachi, C., "Radar Imaging of the Ocean Surface", Boundary-Layer Meteorology, to be published, 1977.

Elachi, C.; T.W. Thompson and D. King, "Observation of the Ocean Wave Pattern Under Hurricane Gloria with an Airborne Synthetic Aperture Radar," Science, to be published, 1977.

Graham, L. 1975, "Flight Planning for Stereo Radar Mapping," Proceedings, 41st Annual Meeting of the Am.Soc. Photogrammetry, Washington, D.C.

Jain, A., "Determination of Ocean Wave Heights from Synthetic Aperture Radar Imagery", Appl. Phys., in press (1977).

Koopmans, B. (1973) "Drainage Analysis on Radar Images, "ITC Jour., 1973-3, Enschede, The Netherlands.

Koopmans, B. (1974) "Should Stereo SLAR Imagery be Preferred to Single Strip Imagery for Thermatic Mapping," ITC Jour., 1974-3, Enschede, The Netherlands.

LaPrade, G.L. (1963) "An Analytical and Experimental Study of Stereo for Radar," Photogrammetric Engineering, Vol. XXIX.

LaPrade, G.L. (1970) "Subjective Considerations for Stereo Radar," Photogramme-

tric Engineering, Vol. XXXVI.

Larson, T.R; L.I. Maskowitz and J.W. Wright, "A Note on SAR Imagery of
    the Ocean, "IEEE Trans. on Antennas and Propagation, Vol.AP-24,
    393,394 (1976).

Leberl, F. (1972) "On Model Formation with Remote Sensing Imagery,"
    Österr. Z. für Vermessungswesen, Nr. 2

Leberl, F. (1976) "Satellitenradargrammetrie", Deutsche Geodätische
    Kommission, Series C., in press

Leberl, F. (1975) "Radargrammetry for Image Interpreters," 2nd Edition,
    ITC, Enschede, Netherlands.

Leberl, F. (1976b) "Mapping of Lunar Surface from Side-Looking Orbital
    Radar Images," The Moon, 15.

Manual of Photogrammetry (1966) "Photogrammetric and Radargrammetric
    Techniques," Vol. II, 3rd Edition, American Society for Photo-
    grammetry, Falls Church, U.S.A.

Phillips, R.J., et al. (1973) "Apollo Lunar Sounder Experiment,"
    Apollo 17 Preliminary Science Report, NASA-SP 330, Washington,
    D.C., U.S.A.

Roessel J.v., R. de Godoy (1974) "SLAR Mosaics for Project RADAM",
    Photogrammetric Engineering, Vol. XL.

Rosenfield, G.H. (1968) "Stereo Radar Techniques," Photogrammetric
    Engineering, Vol. XXXIV.

Rydstrom, H.C. (1968) "Radargrammetric Applications of the Right
    Angle Solution Nomogram," Goodyear Aerospace Corp., Report G1B,
    9124, Litchfield Park, Arizona, U.S.A.

Schaber, G.G.; G.L. Berlin and W.E. Brown, "Variations in Surface
    Roughness within Death Valley, California: Geologic Evaluation of
    25 cm Wavelength Radar Images," Geological Society of America
    Bulletin, Vol. 87, pp. 29-41, 1976.

Schertler, R.J. et al. (1975) "Great Lakes All-Weather Ice Information
    System," Proceedings, 10th Symposium on Remote Scanning of Environ-
    ment, Ann Arbor, Michigan, U.S.A.

Shemdin, O.H.; Brown, Hr., W.E.; Staudhammer, F.G.; Shuchman, R.;
    Rawson, R.; Zelenka, J.; Ross, D.B. and Berles, R.A.,(1977):
    "Some Results of the Marineland Test: Part I., "Boundary-Layer
    Meteorology, to be published.

Super, A.D., et al. (1975) "Remote Sensing Applied to the International
    Ice Patrol", Proceedings, 10th Symposium on Remote Sensing of
    Environment, Ann Arbor, Michigan, U.S.A.

Tiernan, M., et al. (1976) "Lunar Cartography with the Apollo and ALSE
    Radar Imagery," The Moon, Vol. 15.

Wing, R.S., (1970b) "Cholame Area - San Andreas Fault Zone -- California:
    A Study in SLAR", Modern Geology, Vol. 1, No. e, June, pp. 173-186.

Wing, R.S. and L.F. Dellwig, 1970a) "Radar Expression of Virginia
    Dale Precambrian Ring-Dike Complex,Wyoming -- Colorado," Bul. of
    the Geo. Soc. of Amer., Vol. 81, No. 1, January, pp. 293-298.

Wing, R.S.; W.K. Overbey, Jr.,; and L.F. Dellwig, (1970) "Radar Lineament
    Analysis, Burning Springs Area, West Virgina -- An Aid in the
    Definition of Appalachian Plateau Thrusts," Bulletin of the Geologi-
    cal Society of America, Vol. 81, No. 11, November, pp. 3437-3444.